UNIVERSITÄT AUGSBURG
Universitätsbibliothek

OPEN ACCESS
OPUS AUGSBURG

# Lattice modes and the Jahn-Teller ferroelectric transition of GaV4S8

**J. Hlinka, F. Borodavka, I. Rafalovskyi, Z. Docekalova, J. Pokorny, I. Gregora, Vladimir Tsurkan, H. Nakamura, Franz Mayr, Christine A. Kuntscher, Alois Loidl, Sándor Bordács, D. Szaller, H.-J. Lee, J. H. Lee, István Kézsmárki**

**Angaben zur Veröffentlichung / Publication details:**

Hlinka, J., F. Borodavka, I. Rafalovskyi, Z. Docekalova, J. Pokorny, I. Gregora, Vladimir Tsurkan, et al. 2016. "Lattice modes and the Jahn-Teller ferroelectric transition of GaV4S8." *Physical Review B* 94 (6): e060104. https://doi.org/10.1103/PhysRevB.94.060104.

**Nutzungsbedingungen / Terms of use:**

**licgercopyright**

*Dieses Dokument wird unter folgenden Bedingungen zur Verfügung gestellt: / This document is made available under these conditions:*
***Deutsches Urheberrecht***
*Weitere Informationen finden Sie unter: / For more information see:*
*https://www.uni-augsburg.de/de/organisation/bibliothek/publizieren-zitieren-archivieren/publiz/*

PHYSICAL REVIEW B **94**, 060104(R) (2016)

# Lattice modes and the Jahn-Teller ferroelectric transition of $GaV_4S_8$

J. Hlinka,[1,*] F. Borodavka,[1] I. Rafalovskyi,[1] Z. Docekalova,[1] J. Pokorny,[1] I. Gregora,[1] V. Tsurkan,[2,3] H. Nakamura,[4] F. Mayr,[2] C. A. Kuntscher,[5] A. Loidl,[2] S. Bordács,[6] D. Szaller,[6] H.-J. Lee,[7] J. H. Lee,[7] and I. Kézsmárki[2,6]

[1]*Institute of Physics, Academy of Sciences of the Czech Republic, Na Slovance 2, 182 21 Prague 8, Czech Republic*

[2]*Experimental Physics V, Center for Electronic Correlations and Magnetism, University of Augsburg, 86135 Augsburg, Germany*

[3]*Institute of Applied Physics, Academy of Sciences of Moldova, MD 2028, Chisinau, Republic of Moldova*

[4]*Department of Materials Science and Engineering, Kyoto University, Kyoto 606-8501, Japan*

[5]*Experimental Physics II, Center for Electronic Correlations and Magnetism, University of Augsburg, 86135 Augsburg, Germany*

[6]*Department of Physics, Budapest University of Technology and Economics and MTA-BME Lendület Magneto-optical Spectroscopy Research Group, 1111 Budapest, Hungary*

[7]*School of Energy and Chemical Engineering, Ulsan National Institute of Science and Technology (UNIST), Ulsan 44919, Republic of Korea*

(Received 5 July 2016; published 26 August 2016)

Crystal of $GaV_4S_8$, a multiferroic system hosting a Néel-type skyrmion lattice phase, has been investigated by polarized Raman and IR spectroscopy above and below the ferroelectric phase transition. Counts of the observed IR and Raman-active modes belonging to distinct irreducible representations agree quite well with group-theory predictions. Phonon spectra are assigned and interpreted with the aid of *ab initio* calculations of the phonon spectra in the ferroelectric phase. Results allow appreciation of phonon frequencies of the modes involved in Jahn-Teller distortion and their contribution to the spontaneous polarization.

DOI: 10.1103/PhysRevB.94.060104

The ternary chalcogenide $GaV_4S_8$ (GVS) has recently attracted considerable attention due to its multiferroic properties. First of all, the low-temperature zero-field phase of GVS is simultaneously ferroelectric and ferromagnetic up to about $T_{FM} \approx 5$ K. Its magnetization corresponds to $S = 1/2$ per formula unit and its electric polarization is also appreciable ($P_s \approx 1\ \mu C\,cm^{-2}$). Moreover, clear experimental evidence has been found for a sizable magnetoelectric coupling [1]. Secondly, GVS exhibits an interesting magnetic cycloidal order between $T_{FM}$ and $T_N = 13$ K, which can be transformed by a moderate magnetic field (of about 40 mT) into a Néel-type skyrmion lattice (SkL) phase [2]. As predicted in the seminal works of Bogdanov *et al.* [3–5] the important prerequisite for the appearance of this very unusual spin texture (Néel-type SkL) is the polar macroscopic symmetry of the underlying crystal lattice. In GVS, the suitable $C_{3v}$ symmetry emerges together with the ferroelectric polarization below the Jahn-Teller phase transition $T_{JT} = 42$ K [6,7]. This unusual phase transition was shown to be driven by a strong electron-phonon coupling between the unpaired electron in the highest-energy, orbitally degenerate electronic state of the $V_4$ cluster and two corresponding Jahn-Teller-active zone-center modes of the noncentrosymmetric paraelectric structure of GVS [8].

The aim of this Rapid Communication is to explore the role of the zone-center phonon modes in the phase transition using Raman and IR spectroscopy and the *ab initio* approach. In particular, we have (i) determined the spectrum of zone-center phonon modes of GVS, (ii) identified two phonon modes primarily involved in the phase transition, and (iii) related these findings to the Jahn-Teller phase transition and dielectric properties of GVS.

GVS is a lacunar spinel, i.e., it can be presented as a spinel structure lacking every second Ga atom. It can be viewed as a face-centered cubic (fcc) lattice formed of tetrahedral $GaS_4$ and cubane $V_4S_4$ clusters [see Fig. 1(a)]. The paraelectric phase of $GaV_4S_8$ has a noncentrosymmetric cubic ($T_d$) symmetry [6]. The hybridization of the valence states of the vanadium metal ions within the $V_4S_4$ magnetic building blocks leads to one unpaired localized electron occupying a triply degenerate $t_2$ cluster orbital with an overall spin 1/2. The Ga, V, and S atoms are located at 4*a*, 16*e*, and 16*e* Wyckoff positions of the $F\bar{4}3m$ (No. 216) space group, respectively [6]. Group theory predicts $3A_1 + 3E + 3F_1 + 6F_2$ zone-center optic modes, which involves 12 Raman-active optic modes ($3A_1 + 3E + 6F_2$, the $6F_2$ being simultaneously IR active). Under the $F\bar{4}3m > R3m$ symmetry reduction, the $3F_1$ mode gives rise to $3A_2 + 3E$ doublets and $3F_2$ gives rise to $3A_1 + 3E$ doublets so that in total, there are $9A_1 + 3A_2 + 15E$ zone-center modes expected in the ferroelectric $R3m$ (No. 160) phase. Since the macroscopic symmetry lowering ($\bar{4}3m > 3m$ species No. 172 of Ref. [9]) implies the existence of four ferroelastic and ferroelectric domain states, most work has been done in the cubic phase, where the domains do not intervene.

The samples used in this work were prepared from single crystals grown by the chemical vapor transport method as described in Ref. [2]. Raman data were collected using a Renishaw microscope spectrometer [10,11] operated with a 514 nm laser and an ultranarrow notch filter. Reflectivity measurements were performed on naturally grown (111) surfaces of GVS single crystals with near-normal incidence over the spectral range of 220–48 000 $cm^{-1}$ (25 meV–6 eV). Optical conductivity spectra were obtained by Kramers-Kronig transformation.

Selected Raman spectra taken in backscattering geometry from the natural crystal facets with (111), (011), or (001) pseudocubic crystal orientations at 80 K are shown in Fig. 2. These spectra were used to determine mode frequencies collected in Table I. The spectra actually do not change much with the temperature so that in many cases, additional polarized measurements needed for mode assignments were

*hlinka@fzu.cz

 ©2016 American Physical Society

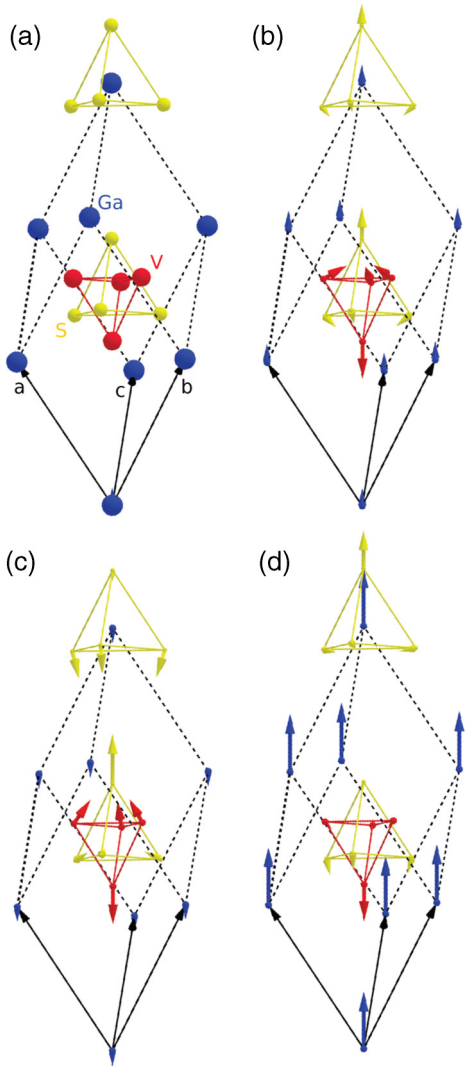


FIG. 1. Rhombohedral crystal structure of GVS with indicated $GaS_4$ and $V_4S_4$ clusters (a) and the *ab initio* predicted eigenvectors of the $A_1[F_2]$ symmetry modes at (c) 203 and (d) 133 $cm^{-1}$ in comparison with the static atomic displacement pattern (b) frozen in the rhombohedral ground state.

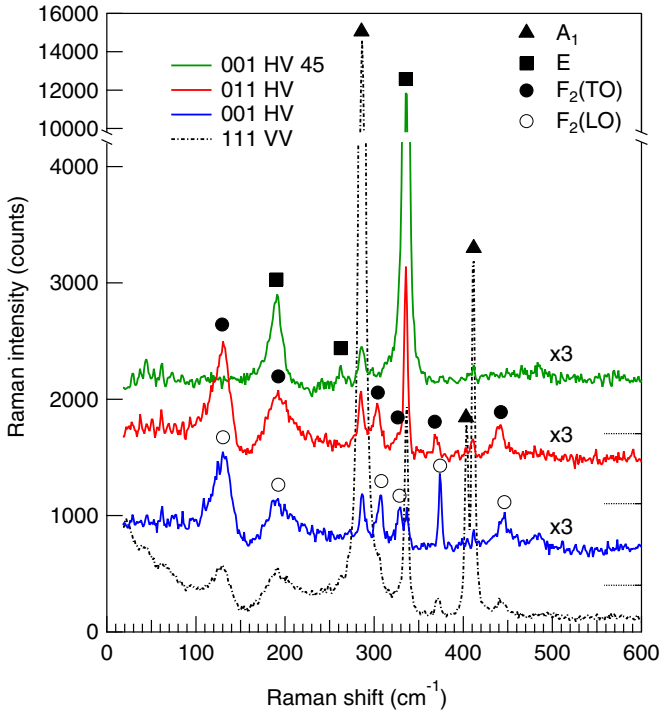


FIG. 2. Polarized Raman spectra of $GaV_4S_8$ single crystal at 80 K (cubic phase) detected in selected experimental configurations. The labels VV and HV in the caption stand for the vertical-vertical and horizontal-vertical orientation of the polarizers in the conventional experiment. More precisely, from top to bottom, the spectra are taken in the cross-polarized backscattering geometry incident to (001) crystal facet with polarizers along [110] and [$\bar{1}$10] (denoted as 001 HV 45), cross-polarized backscattering geometry incident to (011) crystal facet (denoted as 011 HV), cross-polarized backscattering geometry incident to (001) crystal facet with polarizers along [100] and [010] (denoted as 001 HV), and parallel-polarized backscattering geometry incident to (111) crystal facet (denoted as 111 VV).

done at room temperature. The bottom spectrum (111 VV) was recorded in a parallel-polarized configuration from the (111) facet. The three strongest phonon lines near 287, 404, and 411 $cm^{-1}$ were identified as $A_1$ modes. In particular, it was verified on the (001) facet that their parallel-polarized Raman intensity does not change when the polarizers are rotated around the incident beam, what agrees with the form of the $A_1$ Raman tensor of this crystal class [12].

The fourth strong mode in the (111 VV) spectrum was identified as the $E$ symmetry mode (near 336 $cm^{-1}$). Actually, it is the strongest mode in the (001) facet backscattering spectrum, taken with crossed polarizers at $\pm 45^\circ$ with respect to the in-plane pseudocubic directions (the top spectrum in Fig. 2). In this geometry, denoted as (001 HV 45), only the $E$ symmetry modes are allowed. Apart from the leakage scattering of the strongest $A_1$ mode, there are only two other weak modes, at 190 and 263 $cm^{-1}$. These modes were thus also assigned as $E$ modes.

The remaining six lines in the (111 VV) spectrum were identified as the $F_2$ modes. In principle, these modes are also IR active and therefore exist as TO-LO doublets. The LO modes alone should contribute in the (001 HV) spectrum, while the TO modes alone should contribute in the (011 HV) spectrum (middle spectra in Fig. 2). When the (001 HV) and (011 HV) spectra are compared with each other, there is indeed a slight shift between the positions of the modes near 304, 314, 371, and 442 $cm^{-1}$. The two remaining $F_2$ modes, near 130 and 190 $cm^{-1}$, do not show any obvious LO-TO shift, partly because they do not have a strong dynamic dipole moment, but also because they are considerably broadened. Such a spectral broadening in a chemically homogeneous material is usually linked to some kind of lattice anharmonicity or electron-phonon interaction [13–15]. This also indicates that the two lowest frequency $F_2$ phonon modes are the searched Jahn-Teller active modes. Moreover, the characteristic line shape asymmetry suggests that they are mutually coupled, too.

The assignment of the $F_2$ modes near 304, 314, 371, and 442 $cm^{-1}$ was also confirmed by IR spectroscopy (see Fig. 3). The fact that the $F_2$ modes are the only IR-active modes in

TABLE I. Correspondence between the experimentally detected phonon mode frequencies and the *ab initio* calculated mode frequencies of GVS (in $cm^{-1}$). Experimental mode frequencies correspond to the paraelectric cubic phase ($T = 80$ K); the *ab initio* calculated values are in the rhombohedral ground state. However, the rhombohedral distortion is rather weak, so that direct inspection of the phonon mode eigenvectors allows relating them to the parent phase cubic mode representations shown in the first column. Wavenumbers printed in bold correspond to the two $A_1$ modes, contributing most to the frozen ferroelectric distortion of the crystal structure.

| | Raman (80 K) | | IR (80 K) | | Theory (0 K) | | Comment |
|---|---|---|---|---|---|---|---|
| | TO | LO | TO | LO | $E$ | $A_1$ ($A_2$) | |
| $F_2$ | 442 | 445 | 441 | 442 | 440 | 462 | Asym. stretch |
| $A_1$ | 411 | | | | | 419 | $V_4S_4$ breathing |
| $A_1$ | 404 | | | | | 367 | $GaS_4$ breathing |
| $F_2$ | 371 | 374 | 370 | 373 | 336 | 343 | Asym. stretch |
| $E$ | 336 | | | | 338 | | |
| $F_2$ | | 328 | 314 | 326 | 285 | 292 | Strongest IR |
| $F_2$ | 304 | 307 | 303 | 307 | 331 | 326 | |
| $F_1$ | | | | | 305 | (314) | Rotational |
| $A_1$ | 287 | | | | | 287 | Stretch |
| E | 263 | | | | 250 | | |
| $F_1$ | | | | | 220 | (222) | Rotational |
| $F_2$ | 193 | 193 | | | 169 | **203** | $V_4$ JT mode |
| $E$ | 190 | | | | 207 | | |
| $F_1$ | | | | | 142 | (141) | Rotational |
| $F_2$ | 130 | 130 | | | 114 | **133** | Ga-$V_4S_4$ |

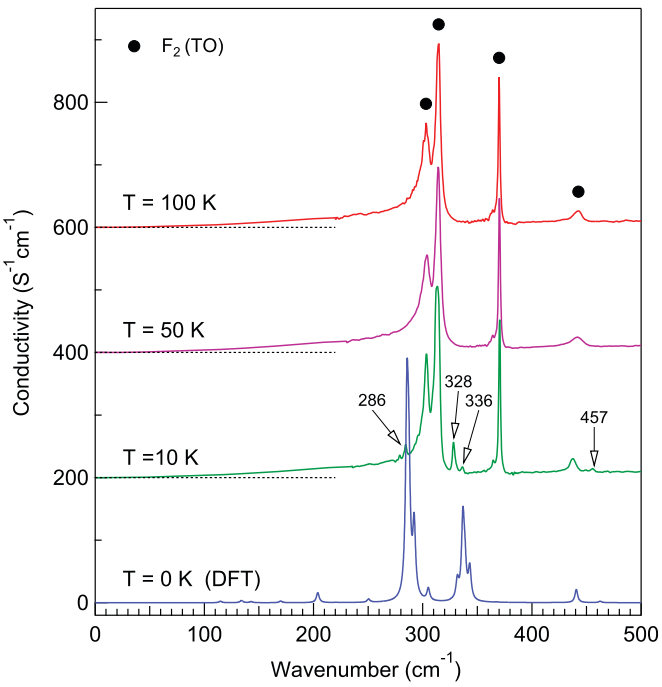


FIG. 3. Spectrum of optical conductivity in the phonon frequency range at selected temperatures. From top to bottom, the spectra correspond to temperatures $T = 100, 50, 10$, and 0 K. The spectrum at 0 K is calculated from damped harmonic oscillators with frequencies and strengths from *ab initio* calculations and with the damping parameter set arbitrarily to $\Gamma = 5\,cm^{-1}$ for all modes. Other spectra are obtained by Kramers-Kronig relations from the directly measured IR reflectivity spectra.

the cubic phase has one important advantage for investigation of the phase transition itself: mode splitting and new modes will necessarily indicate the symmetry lowering. Indeed, the onset of the transition is clearly marked by splitting of the highest-frequency $F_2$ mode into the $A_1 - E$ doublet (437 and 456 $cm^{-1}$ at 10 K) and also by the clear appearance of the additional lines in the conductivity spectra near 286, 336, and 328 $cm^{-1}$, which can be assigned by correspondence with the Raman data as modes derived from the $A_1$, $E$, and $F_1$ modes of the parent cubic phase (the last mode being present in Raman spectra only below $T_{JT}$, as expected from the selection rules). However, a full list of the $9A_1 + 15E$ IR- and Raman-active zone-center modes of the low-temperature phase could not be determined, because of the possible domain twinning and considerable mode overlapping.

Both Raman and IR conductivity spectra have been fitted to a model of independent damped harmonic oscillators (DHO). There is almost no change of the peak positions above 50 K with temperature, only a slight increase of the damping parameters.

In order to obtain insight into the nature of the observed phonon modes, phonon frequencies, eigenvectors, and dynamical charges were also calculated using the *ab initio* approach. Technically, these calculations were performed using density functional theory within the generalized gradient approximation GGA + $U$ method [16] with the local-density approximation as implemented in the Vienna Ab Initio Simulation Package [17,18]. We use the Dudarev [19] implementation with on-site Coulomb interaction $U_{eff} = 2.0$ eV to treat the localized $3d$ electron states of V atoms. The value of $U_{eff}$ reproduces well the experimental magnetic moment of $\approx 1\mu_B$ per $V_4$ unit. The projector augmented wave potentials [20] explicitly include 13 valence electrons for Ga ($3d^{10}4s^24p^1$), six for S ($3s^23p^4$), and 11 for V ($3p^63d^44s^1$). Internal atoms were relaxed within experimental lattice vectors until the residual Hellman-Feynman forces were less than 1.0 meV/Å. The zone-center phonon frequencies of the structures were computed using the frozen phonon method in 13 atoms primitive unit-cell supercells and $6 \times 6 \times 6$ Monkhorst-Pack $k$-point meshes. Spin-orbit coupling was not included. We obtained the modes at $q = 0$ by uniformly displacing all atoms related by translation symmetries of the primitive $GaV_4S_8$ structure. Born effective charges for the relaxed structure were computed by the Berry-phase method [21].

The unit-cell volume (224.3 $Å^3$ per formula unit) and the rhombohedral angle ($\alpha_{rh} = 59.64$) were fixed close to the reported experimental values [6]. Relaxation of the internal parameters resulted in a structure matching nicely the known structural data [6]. Moreover, the resulting spontaneous polarization ($P_s = 2.6\mu$ C/cm$^2$), calculated from the frozen polar phonon modes and the Born effective charges, corresponds well to that of the earlier *ab initio* calculations of Ref. [8] ($P_s = 2.4\mu$ C/cm$^2$) and it is also consistent with the $P_s \approx 0.6\mu$ C/cm$^2$ value determined from the pyroelectric experiments of Ref. [1] (considering, for example, the possibility that the sample measured there could have been in a multidomain, incompletely poled state). Interestingly, the asymmetric stretching of the $V_4$ cluster alone would lead to even larger polarization ($P_s = 3.2\mu$ C/cm$^2$), which implies that the total value is somewhat counterbalanced by the contributions of other frozen

polar modes. On the other hand, the complete ordering of the dynamical dipoles of $V_4$ clusters, estimated from the paraelectric Curie constant, would contribute only little ($P_s = 0.7\mu$ C/cm$^2$). Since the transition is of a first-order nature [22,23], this difference is nevertheless well understandable.

The TO mode phonon frequencies, calculated for the experimental unit cell [6], are listed in Table I. Association with the zone-center modes of the cubic phase has been made by a direct inspection of the phonon eigenvectors. The examples of the phonon eigenvectors of the two lowest frequency $A_1[F_2]$ symmetry modes are shown in Fig. 1. Roughly speaking, the center of mass of the anion subsystem vibrates in-phase with that of cations in the 133 cm$^{-1}$ mode. In the 203 cm$^{-1}$ mode, the center of mass of the anion subsystem does not vibrate much, and the same holds for the cations. Therefore, none of these two modes is expected to show a marked IR activity. This is also consistent with the optical conductivity spectra of Fig. 3. The nature of the other eigenvectors is indicated in the last column of Table I. In general, the level of the agreement between the calculation and the experiment is similar to that reached, e.g., in the recent studies of $BiFeO_3$ phonons [24,25].

In addition, we have used Born effective charges and the calculated eigenvectors to evaluate the mode plasma frequencies as well as the optical conductivity spectrum [26] (assuming a model of independent DHO oscillators with a common damping constant of 5 cm$^{-1}$ for phonon modes and an experimental value of the background permittivity $\epsilon_\infty = 14$). The resulting mode conductivity spectrum, displayed as the bottom spectrum in Fig. 3, agrees qualitatively with the experimental one in the sense that there are the two most pronounced IR bands in the spectrum, one near 300 and the other near 370 cm$^{-1}$, while the modes with frequency below 250 cm$^{-1}$ have only very small dielectric strengths.

The ferroelectric structure can be expressed as the reference cubic structure perturbed by the frozen phonon modes. By comparison of the $F_2$ symmetry part of the frozen structural distortion with the calculated eigenvectors, we have verified that the distortion has the largest overlap with the lowest frequency $A_1[F_2]$ symmetry modes shown in Fig. 1 (at 133 and 203 cm$^{-1}$ in Table I). These modes clearly involve the anticipated Jahn-Teller distortion of the $V_4$ unit as well as the Ga-$V_4S_4$ beating mode. Thus, as concerns the Jahn-Teller ferroelectricity, both experiment and calculations point towards the two lowest frequency $F_2$ phonon modes.

Relatively high frequencies of these two modes suggest that the energy barriers for a homogeneous switching between equivalent domain states are probably higher than $kT_{JT}$, i.e., that the phase transition is of order-disorder type [27]. This is also corroborated by rather small temperature variations of the frequencies of these modes—no clear softening was observed. Therefore, it is very likely that the critically slowing down THz-range relaxational dynamics, observed above $T_{JT}$ in Ref. [7], is simply related to the stochastic jumps of the local Jahn-Teller coordinate among the four equivalent Jahn-Teller potential minima. This is what is actually expected in the canonical picture of the dynamical Jahn-Teller effect. Conceptually, this case is very similar to the order-disorder dynamics known, for example, from $BaTiO_3$ type ferroelectrics [28–30], even though the electronic mechanism behind and the shape of the local potential associated with the dynamical Jahn-Teller effect are obviously very different from that of $BaTiO_3$ type ferroelectrics.

In summary, this polarized Raman and IR spectroscopic study complemented by *ab initio* calculations provides a comprehensive description of the phonon spectra of GVS as well as the clarification of the dynamic nature of the Jahn-Teller phase transition in this model compound.

The work was supported by the Czech Science Foundation (Project GACR 13-15110S) and by the Deutsche Forschungsgemeinschaft via the collaborative research center TRR 80 (Augsburg, Munich, Stuttgart). D.Sz., S.B., and I.K. were supported by Hungarian Research Funds OTKA K 108918, PD 111756, and Bolyai 00565/14/11. J.H.L. was supported by the National Research Foundation of Korea (NRF) grant funded by the Korea government (MSIP) (Grant No. 2.150639.01). D. Sz. was supported by the Hungarian Ministry of Human Resources (New National Excellence Program, UNKP-16-3/III).

[1] E. Ruff, S. Widmann, P. Lunkenheimer, V. Tsurkan, S. Bordács, I. Kézsmárki, and A. Loidl, Sci. Adv. **1**, e1500916 (2015).

[2] I. Kézsmárki, S. Bordács, P. Milde, E. Neuber, L. M. Eng, J. S. White, H. M. Ronnow, C. D. Dewhurst, M. Mochizuki, K. Yanai, H. Nakamura, D. Ehlers, V. Tsurkan, and A. Loidl, Nat. Mater. **14**, 1116 (2015).

[3] A. N. Bogdanov and D. A. Yablonskii, Zh. Eksp. Teor. Fiz. **95**, 178 (1989).

[4] A. Bogdanov and A. Hubert, J. Magn. Magn. Mater. **138**, 255 (1994).

[5] A. Bogdanov and A. Hubert, Phys. Status Solidi B **186**, 527 (1994).

[6] R. Pocha, D. Johrendt, and R. Pöttgen, Chem. Mater. **12**, 2882 (2000).

[7] Z. Wang, E. Ruff, M. Schmidt, V. Tsurkan, I. Kézsmárki, P. Lunkenheimer, and A. Loidl, Phys. Rev. Lett. **115**, 207601 (2015).

[8] K. Xu and H. J. Xiang, Phys. Rev. B **92**, 121112(R) (2015).

[9] J. Hlinka, J. Privratska, P. Ondrejkovic, and V. Janovec, Phys. Rev. Lett. **116**, 177602 (2016).

[10] J. Hlinka, I. Gregora, J. Pokorny, C. Hérold, N. Emery, J. F. Mareché, and P. Lagrange, Phys. Rev. B **76**, 144512 (2007).

[11] F. Borodavka, I. Gregora, A. Bartasyte, S. Margueron, V. Plausinaitiene, A. Abrutis, and J. Hlinka, J. Appl. Phys. **113**, 187216 (2013).

[12] I. Gregora, Raman scattering, in *International Tables for Crystallography* (The International Union for Crystallography, Springer Netherlands, 2006), Chap. 2.3, Vol. D.

[13] J. Hlinka, I. Gregora, J. Pokorny, A. Plecenik, P. Kus, L. Satrapinsky, and S. Benacka, Phys. Rev. B **64**, 140503(R) (2001).

[14] T. Yildirim, O. Gülseren, J. W. Lynn, C. M. Brown, T. J. Udovic, Q. Huang, N. Rogado, K. A. Regan, M. A. Hayward, J. S. Slusky, T. He, M. K. Haas, P. Khalifah, K. Inumaru, and R. J. Cava, Phys. Rev. Lett. **87**, 037001 (2001).

[15] E. Cappelluti, Phys. Rev. B **73**, 140505(R) (2006).

[16] C. Loschen, J. Carrasco, K. M. Neyman, and F. Illas, Phys. Rev. B **75**, 035115 (2007).
[17] G. Kresse and J. Hafner, Phys. Rev. B **47**, 558(R) (1993).
[18] G. Kresse and J. Furthmüller, Phys. Rev. B **54**, 11169 (1996).
[19] S. L. Dudarev, G. A. Botton, S. Y. Savrasov, C. J. Humphreys, and A. P. Sutton, Phys. Rev. B **57**, 1505 (1998).
[20] P. E. Blochl, Phys. Rev. B **50**, 17953 (1994); G. Kresse and D. Joubert, *ibid.* **59**, 1758 (1999).
[21] R. D. King-Smith and D. Vanderbilt, Phys. Rev. B **47**, 1651 (1993).
[22] S. Widmann, E. Ruff, A. Günther, H.-A. Krug von Nidda, P. Lunkenheimer, V. Tsurkan, S. Bordács, I. Kézsmárki, and A. Loidl, arXiv:1606.04511.
[23] M. E. Lines and A. M. Glass, *Principles and Applications of Ferroelectrics and Related Materials* (Oxford University Press, New York, 1977).
[24] J. Hlinka, J. Pokorny, S. Karimi, and I. M. Reaney, Phys. Rev. B **83**, 020101 (2011).
[25] M. Goffinet, P. Hermet, D. I. Bilc, and Ph. Ghosez, Phys. Rev. B **79**, 014403 (2009).
[26] J. Hlinka, J. Petzelt, S. Kamba, D. Noujni, and T. Ostapchuk, Phase Transitions **79**, 41 (2006).
[27] J. Hlinka, T. Janssen, and V. Dvořák, J. Phys.: Condens. Matter **11**, 3209 (1999).
[28] R. Pirc and R. Blinc, Phys. Rev. B **70**, 134107 (2004).
[29] J. Hlinka, T. Ostapchuk, D. Nuzhnyy, J. Petzelt, P. Kuzel, C. Kadlec, P. Vanek, I. Ponomareva, and L. Bellaiche, Phys. Rev. Lett. **101**, 167402 (2008).
[30] J. Weerasinghe, L. Bellaiche, T. Ostapchuk, P. Kužel, C. Kadlec, S. Lisenkov, I. Ponomareva, and J. Hlinka, MRS Commun. **3**, 41 (2013).